ACS Catalysis

Research Article

pubs.acs.org/acscatalysis

# Coupling Titania Nanotubes and Carbon Nanotubes To Create Photocatalytic Nanocomposites

Baiju K. Vijayan,[†,‡,#] Nada M. Dimitrijevic,[§,⊥] Daniel Finkelstein-Shapiro,[‡,∥] Jinsong Wu,[¶,□] and Kimberly A. Gray*[,†,‡]

[†]Institute of Catalysis for Energy Processes, Center for Catalysis and Surface Science, [‡]Department of Civil & Environmental Engineering, [∥]Department of Chemistry, [¶]Department of Materials Science and Engineering, and [□]The NUANCE Center, Northwestern University, Evanston, Illinois 60208, United States

[§]Chemical Sciences and Engineering Division [⊥]Center for Nanoscale Materials, Argonne National Laboratory, Illinois 60439, United States

Supporting Information

**ABSTRACT:** A titania nanotube/single-wall carbon nanotube composite was prepared by a simple hydration dehydration process. These composites were characterized using X-ray diffraction and spectroscopic techniques (UV−visible diffuse reflectance, Raman, photoluminescence, and EPR) as well as electron microscopy (SEM, TEM). SEM and TEM images indicated that single-wall carbon nanotubes (SWCNTs) were interwoven with the titania nanotubes. Raman spectra further confirmed the chemical interaction between the titania nanotube and the SWCNT in the composites. The photoactivity of these composites was tested by the photooxidation of acetaldehyde. The composites showed enhanced photoactivity under both visible and UV light in comparison with conventional titania (P25) and controls. The composite having a mass ratio of 1:50 (SWCNT/TiNT) showed the maximum photocatalytic activity for acetaldehyde decay under visible light. XPS and EPR spectra indicated the creation of Ti−O−C bonds between the titania nanotube and the SWCNTs during the hydration dehydration process, which explains the visible light photoactivity.

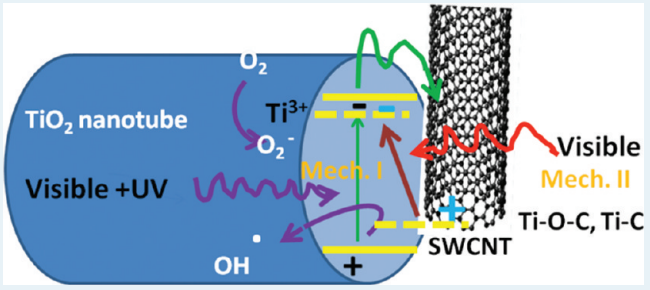


**KEYWORDS:** *titania nanotube, carbon nanotube, photocatalysis*

## INTRODUCTION

Titania nanotubes have attracted growing interest for environmental and energy applications because of their structure-dependent enhanced photoelectronic properties.[1−5] Irradiating titania with photons having an energy larger than the bandgap, normally in the UV region, excites electrons to the conduction band, leaving a charge vacancy in the valence band. Upon migration to the catalyst surface, these charges are capable of driving oxidizing and reducing reactions, although the rapid recombination of the photoinduced charges is a persistent phenomenon significantly diminishing the photoefficiency of the system. Two major challenges associated with photocatalysis are to decrease the recombination rate and red-shift the photoresponse to the visible region. Various techniques to tackle these challenges have been adopted and include (1) doping with cations and anions, (2) doping with noble metals, and (3) coupling with narrow-band-gap semiconductors.[6−9]

Titania nanocomposites created by linking titania with single-wall carbon nanotubes (SWCNTs) have also recently been found to hold promise along these lines.[10−20] Carbon nanotubes (CNTs) enhance the photoactivity in three different ways by (1) acting as a sink for electrons to enhance the lifetime of separated charges; (2) serving as a surface impurity dopant, creating band gap energy states; and/or (3) forming Ti−O−C or Ti−C defect sites that enable visible light absorption and photocatalysis.[21,22]

Mishra and co-workers reported the potential use of CNT/titania nanotube (TiNT) composites prepared through anodization process for hydrogen storage applications.[10] CNTs grown on the surface of TiNT prepared through anodization was effectively used as a catalyst in electrooxidation of methanol.[11] Aligned carbon nanotubes (CNTs) were used as a template for the preparation of titania nanotube arrays.[12] Sun et al. prepared titania nanoparticle/CNT composites by the direct hydrolysis method.[13] Using a sol−gel method, Gao synthesized a titania/CNT composite, which showed enhanced photooxidation of methylene blue.[14] Wang and co-workers also reported photocatalytic improvements for the photooxidation of phenol by titania/MWCNT composites made with a sol−gel method.[15] An and co-workers prepared a titania/MWCNT composite using a supercritical ethanol technique to improve phenol degradation.[16] The photoinactivation of *Escherichia coli* using titania deposited

Received: October 20, 2011
Revised: December 20, 2011
Published: December 27, 2011

  

on vertically aligned MWCNT was demonstrated by Akhavan et al.[17] Yuan Gao employed a titania/CNT hybrid catalyst for the photocatalytic decomposition of acridine dye.[18] Llobet et al. studied the oxygen sensing properties of a titania/CNT thin film.[19]

In this research, TiNT/SWCNT composites in different mass ratios are fabricated using a simple hydration−dehydration method and then are thoroughly characterized by X-ray diffraction (XRD), UV−visible diffuse reflectance spectroscopy, scanning electron microscopy (SEM), transmission electron microscopy (TEM), and Raman spectroscopy. Their photoactivity is compared by following the decay of acetaldehyde under UV and visible light. Electron paramagnetic resonance spectroscopy (EPR) and photoluminescence spectroscopy (PL) are used to characterize further the optical and electronic properties of the materials and to explain differences in their catalytic activity.

## EXPERIMENTAL SECTION

Titania nanotubes were prepared by a modified hydrothermal method reported previously.[23−26] In a typical experiment, 2 g of anatase titania powder (assay 99%, Sigma Aldrich Chemicals, USA) was stirred with 50 mL of 10 M NaOH solution (assay 97%, BDH Chemicals, USA) in a 125 mL Teflon cup. The Teflon cup was kept in an oven for 48 h maintained at 120 °C, and the resultant precipitate was washed with 1 M HCl (assay 38%, EMD Chemicals, USA), followed by several washings using deionized water to attain a pH between 6 and 7. The titania nanotube powder thus formed was dried in an oven at 110 °C overnight, followed by calcination under hydrogen atmosphere (80 mL $min^{-1}$) at 400 °C for 1 h. The TEM image of the as-prepared TiNTs is provided in the Supporting Information (Figure S1). SWCNTs synthesized by an electric arc discharge method (Carbon Solutions, Inc.) were treated in our laboratory using a reflux system with concentrated nitric acid (70%) at ∼150 °C for 1 h to remove the Ni/Y catalyst and amorphous carbon impurities.[20,27,28] In general, acid treatment of SWCNTs tends to functionalize the nanotube walls with carboxyl groups, which enhances the adsorption of $TiO_2$ or organic compounds on the SWCNTs.[29]

TiNT/SWCNT composite nanostructures were prepared by a simple evaporation and drying process.[20] First, ∼10 mg of purified SWCNTs was dispersed in water in a 150 mL beaker and sonicated for 10 min. TiNT powder was added to the suspension while stirring. After additional sonication for 10 min, the suspension containing SWCNTs and TiNT powders was heated to 80 °C on a stir plate with air flowing across the suspension's surface to accelerate the evaporation of water. After the water evaporated, the composite was dried overnight in an oven at 110 °C to avoid oxidation of the SWCNTs that occurs at higher temperatures in the presence of oxygen. Composites were made at TiNT/SWCNT mass ratios of 20:1, 50:1, and 100:1 in batches of ∼200 mg. They are named TiNT, 20TiNT, 50TiNT, and 100TiNT, respectively, in the following tests.

XRD patterns of the samples were taken in a Rigaku X-ray diffractometer in the diffraction angle 2$\theta$ range 5−80° using Cu K$\alpha$ radiation. The morphology of TiNT was observed by SEM (Hitachi S-4800-II) and TEM (Hitachi HD-2300A). Raman spectra were recorded on a FT Raman spectrometer (Acton TriVista CRS Confocal Raman System, Princeton Instruments, USA). The photoluminesence of the TiNT composite powder was measured with a photon-counting fluorescence spectrometer (ISS PC1). The material was packed into a pellet, and the chamber was purged with nitrogen 30 min prior to and throughout the measurement to reduce nonradiative quenching due to oxygen. Vertically polarized light at 300 nm was used for excitation, and the photoluminescence was collected at horizontal polarization in a reflection geometry. The correction to the measured intensity due to the composite absorption of visible light is detailed in the Supporting Information.

The photoactivity of the composites was studied using acetaldehyde photodegradation. For photocatalytic reaction tests, 10 mg of TiNT/SWCNT composite powders and controls were placed in a photocatalytic system consisting of a closed square Teflon container having a quartz window.[8] To determine if TiNTs improved titania reactivity, a powder sample of Evonik-Degussa P25 was also tested. Into the closed, dark chamber, 1 mL of saturated vapor of acetaldehyde was introduced and kept for 1 h for equilibration. Photocatalytic reactions were carried out by irradiation with a xenon lamp with and without a 450 nm filter and a natural daylight bulb (60 W) having energy densities of ∼73, 55, and 31 $W/m^2$, respectively (the emission spectra of the lamps are illustrated in Figure S2, Supporting Information). As the photocatalytic reaction proceeded, the degradation of acetaldehyde was monitored at different time intervals using an HP 5890 gas chromatograph equipped with a flame ionization detector (GC−FID). EPR spectra were collected on a Bruker Elexys E580 spectrometer equipped with a helium cryostat. For the characterization of photogenerated charges, samples dispersed in Milli-Q water were purged with argon and illuminated within the cavity while spectra were acquired.[30,31] A 300 W xenon lamp (ILC Inc.) was used as the light source for EPR studies. The $g$ tensor values were calibrated for homogeneity and accuracy by comparing with a coal standard ($g$ = 2.002 85 ± 0.000 05).

## RESULT AND DISCUSSIONS

The XRD spectra of the TiNT and TiNT/SWCNT composite are presented in Figure 1. The TiNT has a XRD pattern that

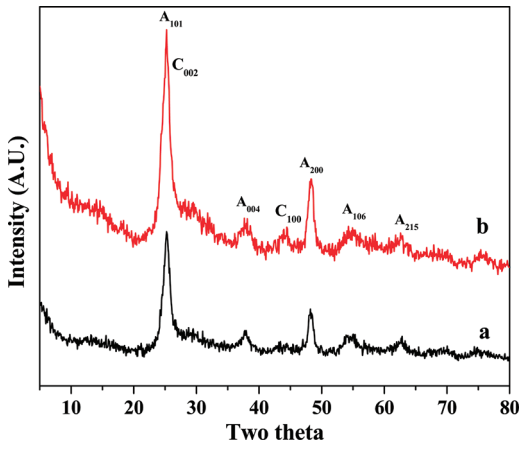


**Figure 1.** XRD pattern of (a) titania nanotube and (b) titania nanotube/SWCNT composite (1:20 mass ratio).

corresponds to the anatase crystal phase of titania (Figure 1a). The peak at a 2 $\theta$ value of 13.3 in the XRD spectra corresponds to the reflection from the TiNT wall; that is, the TiNT are formed by rolling a titania layer formed in the hydrothermal process.[32] X-ray reflections of the anatase crystal phase (JCPDS 21-1272) at 2$\theta$ = 25.3°, 37.7°, 48.3° were observed in pure


dx.doi.org/10.1021/cs200541a | ACS Catal. 2012, 2, 223−229

TiNT and TiNT/SWCNT composites. A weak Bragg peak in the functionalized SWCNT at the positions of $2\theta = 43.76°$ can be indexed as (100) diffractions, which are characteristic of SWCNTs and correspond to the graphitic nature of the SWCNT (Figure 1b).[33−35]

The diffuse reflectance UV−vis spectra of the composite catalysts, expressed in terms of Kubelka−Munk equivalent absorption units, are presented in Figure 2. As expected, the

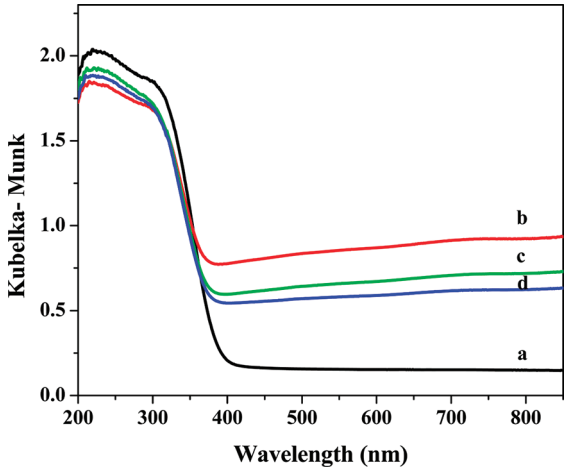


**Figure 2.** Absorbance spectra of SWCNT and titania nanotube/SWCNT composites at different mass ratios: (a) TiNT, (b) 1: 20, (c) 1:50, and (d) 1: 100.

TiNTs have no absorption above the fundamental absorption sharp edge rising at 385 nm. In contrast, the TiNT/SWCNT composite catalysts absorb at longer wavelengths than that of TiNT alone. An apparent enhancement of absorption is observed even for the composite catalyst with very small mass ratio of the SWCNT (1:100), and for all composites, the enhanced absorbance extends broadly over wavelengths >400 nm. The absorbance increased in direct proportion to the mass of SWCNT in the composites. This is in contrast to the observations of Arana et al.,[36] who found no correlation in the UV−visible spectra as a function of the activated carbon/titania composite ratio.

The morphology of TiNT/SWCNT composites was studied using SEM, as shown in Figure 3. The SEM images indicate

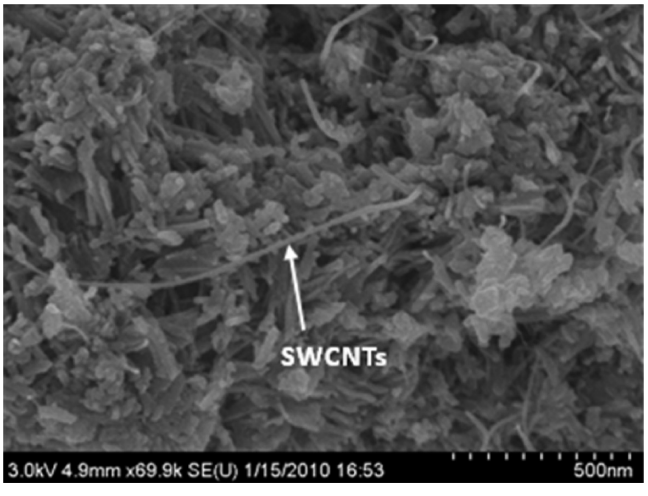


**Figure 3.** SEM images of the titania nanotube/SWCNT composite.

that the SWCNTs are homogenously distributed throughout the TiNT matrix. The titania nanotubes of length 50−300 nm are interwoven with the longer SWCNTs, and the corresponding areas are marked in Figure 3. TEM results, illustrated in Figure 4, not only are consistent with the SEM results, but also

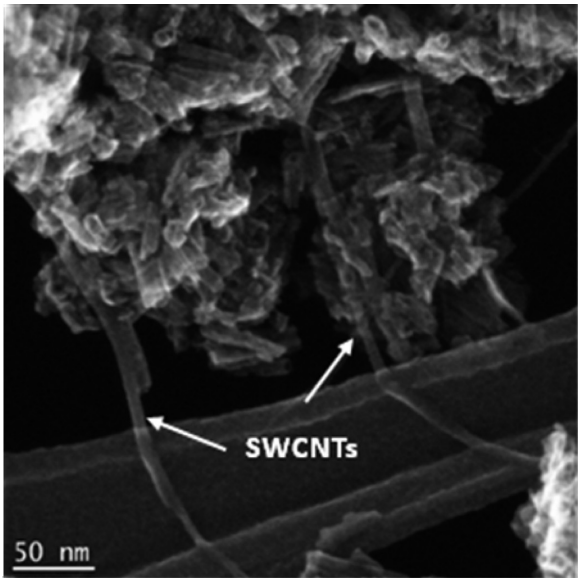


**Figure 4.** STEM image of titania nanotube/SWCNT composite collected on a HD2300 STEM using a secondary electron detector.

show more clearly that the SWCNTs are interwoven between the TiNTs, providing direct interaction between TiNTs and SWCNTs.

Raman spectroscopy was used to interrogate the interaction of the titania nanotube with the SWCNTs. The spectra of the SWCNT, TiNT, and TiNT/SWCNT composite are illustrated in Figure 5. The characteristics peaks at 149, 198, 396, 510, and

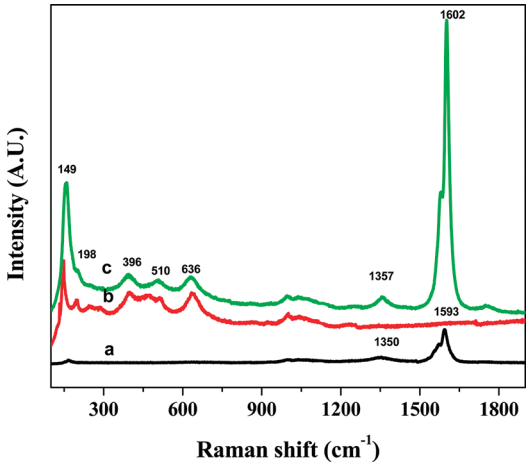


**Figure 5.** Raman spectra of (a) SWCNTs, (b) titania nanotube, and (c) TiNT/SWCNTs composite (1:20).

636 $cm^{-1}$ correspond to the anatase phase of titania, confirming that the TiNT crystal phase remains unchanged in the composite. The composite sample (spectrum c in Figure 5) shows the D,G and RBM bands of SWCNTs.[37] The D and G bands of the SWCNT (spectrum a in Figure 5) are observed at 1350 and 1593 $cm^{-1}$, respectively. These bands shift to 1357 and


dx.doi.org/10.1021/cs200541a | ACS Catal. 2012, 2, 223−229

1602 $cm^{-1}$ in the TiNT/SWCNT composite, clearly indicating that the strong interaction between the TiNT and the SWCNT[38] could enhance charge transfer from the TiNT to the SWCNT to separate and stabilize the charge and thereby hinder charge recombination.

The XPS spectra of the carbon 1s peak in the SWCNTs and the TiNT/SWCNT composite are provided in Figure 6A, B, and C. The peak corresponding to 284.5 eV is related to the $sp^2$ hybridized carbon in the SWCNT. Additional peaks are observed in the sample around 285.6 and 288.7 eV, which correspond to the carbon attached to oxygen atoms and reflect the formation of defects in the SWCNTs during their purification using concentrated $HNO_3$. These defects are attributed to the >C−O− (alcoholic) or −COO− (carboxylic acid, ester) moieties[38,39] and can easily bind to the surface hydroxyl group of titania, forming Ti−O−C bonds, which impart visible light activity to the titania. In addition to these peaks, the TiNT/SWCNT composite bears an additional peak at 283.6 eV, indicating the Ti−C bond (Figure 6C).[40,41] In the present study, the hydration−dehydration process enables the formation of these bonds in the composites and leads to visible light photoactivity. The strong absorption in the visible range (Figure 2) of the TiNT/SWCNT composites confirms this. Others have reported that annealing temperatures such as 400 °C are needed for the formation of such bonds.[42] Yet, we find that such bonds form by the hydration−dehydration process. It is also reported that carboxylic acid groups adsorb strongly onto bare titanium dioxide surfaces,[43] and this, too, may account for the formation of Ti−O−C bonds in the hydration−dehydration process.

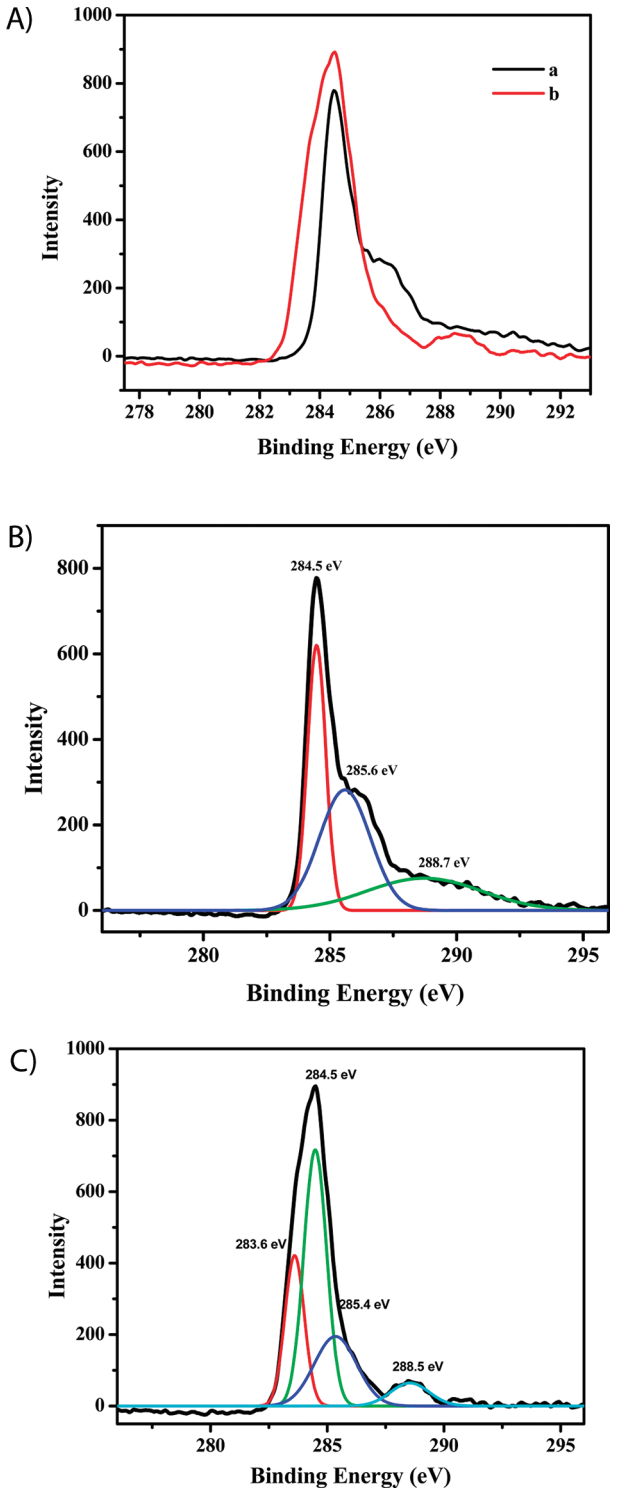


**Figure 6.** XPS spectra of (A) carbon peak (a) SWCNTs purified, (b) TiNT/SWCNT composite (1:20), (B) spectral decomposition of the purified SWCNTs carbon peak, and (C) spectal decomposition of the TiNT/SWCNT composite carbon peak.

The photoluminescence (PL) was measured for samples with varying ratios of SWCNT to TiNT according to the synthesis method described earlier, as well as for a mechanical mixture of 1:50 SWCNT/TiNT. The emission peaks of the TiNTs are illustrated in Figure 7 and Table 1 in the Supporting Information. We observe that the PL is strongly quenched in the presence of the SWCNTs, which is consistent with electron transfer from the conduction band of $TiO_2$ to the nanotubes.[44] The lower intensity for 1:50 relative to that of the 1:50 mechanically mixed material indicates that there is a stronger electronic coupling created during the hydration−dehydration process.

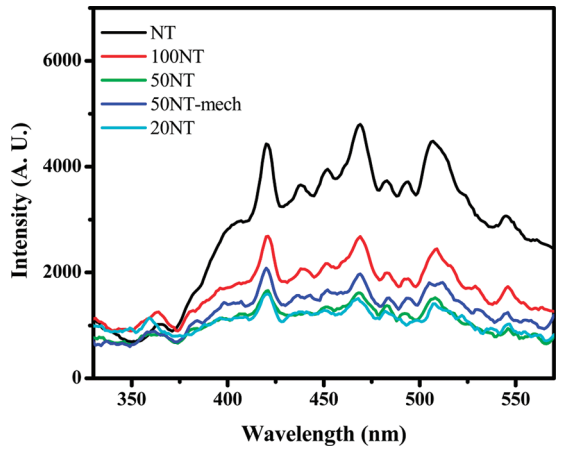


**Figure 7.** Photoluminescence at 300 nm excitation normalized by the absorbance.

The photooxidation of the acetaldehyde is measured to probe how coupling TiNTs to SWCNT affects photocatalysis. The photocatalytic oxidation of gaseous acetaldehyde by $TiO_2$ is driven by active oxygen species resulting from the trapping of photogenerated electrons by oxygen or the trapping of photogenerated holes by hydroxyl groups on the titania surface. This radical chain reaction in the presence of oxygen occurs in two possible pathways: (1) direct reaction of acetaldehyde to


dx.doi.org/10.1021/cs200541a | ACS Catal. 2012, 2, 223−229

carbon dioxide (eq 1) or (2) through the formation of acetic acid as an intermediate, which is then oxidized into $CO_2$ (eqs 2, 3).[45,46]

$$2CH_3CHO + 2^{\bullet}OH + O_2 \rightarrow 2CH_3^{\bullet} + 2CO_2 + 2H_2O \quad (1)$$

$$CH_3CHO + {}^{\bullet}OH + O_2 \rightarrow CH_3COOH + HOO^{\bullet} \quad (2)$$

$$CH_3COOH + h^+ \rightarrow CO_2 + CH_3^{\bullet} + H^+ \quad (3)$$

In this study, we have detected trace amounts of acetic acid as an intermediate but have not quantified it because it does not accumulate and is rapidly degraded. Three different sources of light were used for the reaction: (a) xenon lamp, which provides light with wavelengths >200 nm (Supporting Information Figure S2); (b) xenon lamp with 450 nm filter, which eliminates all the light below 450 nm; and (c) a low-intensity natural daylight lamp, which is commonly used for household lighting applications. Although the xenon lamp without filter has photons energetic enough to photolyze acetaldehyde to $CO_2$ (see Supporting Information), this does not affect the trends observed in the study.

Under all illumination conditions tested, the SWCNT/TiNT composites show greater photocatalytic activity than the bare TiNT and, in most cases, P25 (Figure 8). Under UV irradiation with the xenon lamp, the degradation rate follows the order 20NT > 50NT > 100NT > P25 > NT (Figure 8A). This is in agreement with the degree of quenching observed in photoluminescence. Acetaldehyde decay under visible light sources is also illustrated for these materials in Figure 8B, C. Assuming a pseudo-first-order reaction for the oxidation, we compare photocatalytic reaction rates under all irradiation conditions in Figure 9. The photoreactivity of the TiNT and the composites follows the order of photocatalytic reactivity 50NT > 100NT > 20NT > NT > P25 under the filtered xenon source and natural daylight bulb.

Although the TiNT/SWCNT composites showed considerable enhancement of acetaldehyde degradation under all conditions, especially under visible light excitation, the explanation of the improvement differs depending on the conditions of photoexcitation. A schematic of the proposed mechanisms is presented in Supporting Information Figure 6. Under UV excitation, the photoexcited electrons on the titania transfer to the SWCNTs, resulting in greater charge separation and hindered recombination. The emission quenching in PL spectra is consistent with these events. Gao et al.[20] observed that there is a specific relationship between the coverage of the titania nanoparticles by SWCNTs, which affects the photoactivity of the composite. The SEM and TEM images show the individual contact between TiNT/SWCNTs (Figures 3, 4). Under the UV irradiation, the SWCNTs act as electron acceptors while the titania nanotube act as electron donors. The hole remains on the titania and is trapped at surface hydroxyls, creating highly reactive hydroxyl radicals.

In contrast, under visible light condition (xenon lamp with 450 nm filter and natural daylight bulb), different mechanisms are at play. In previous work, we have shown that oxygen vacancies and $Ti^{3+}$ are formed when the TiNT are calcined under a hydrogen atmosphere.[8] These defects produce a red shift and account for the visible light photoactivity of the TiNTs alone.[47,48] The improved visible photoactivity of the TiNT/SWCNT composites, however, is explained by the formation of Ti−C and Ti−O−C defect sites that not only effectively narrow the band gap of the TiNT but also may serve as trapping sites to retard recombination. Previous reports indicate that the Ti−O−C bond formed by the TiNT/SWCNT coupling leads to the visible light activity.[17,21,41]

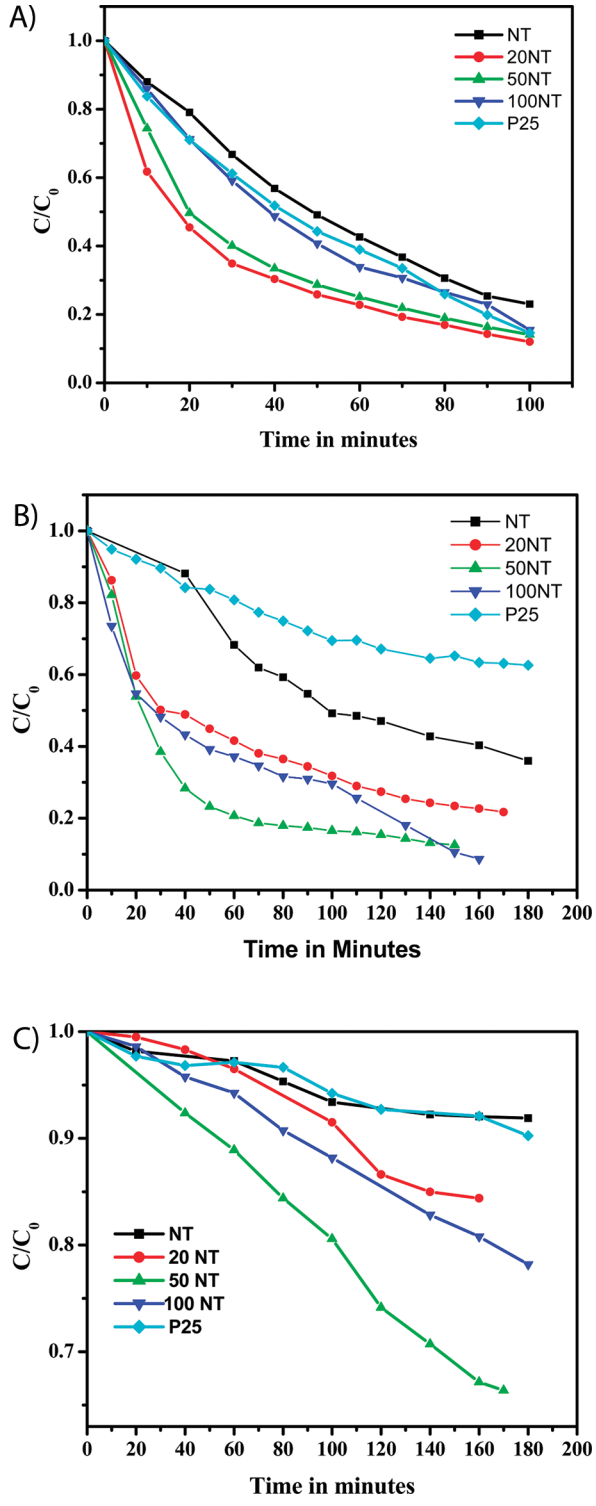


**Figure 8.** Photodegradation of acetaldehyde: (A) xenon lamp, (B) xenon lamp with 450 nm filter, and (C) natural daylight bulb.

In addition, Wang et al[15] proposed that CNTs may sensitize the TiNT under the visible light and transfer the excited electrons to midgap states on titania, possibly the Ti−C or Ti−O−C trapping sites. The positively charged carbon nanotube then


dx.doi.org/10.1021/cs200541a | ACS Catal. 2012, 2, 223−229

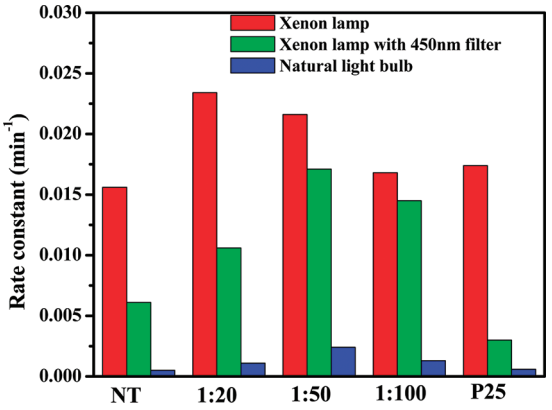


**Figure 9.** Comparison of rate constants for the photocatalytic degradation of acetaldehyde under various illumination conditions by assuming pseudo-first-order reaction.

abstracts an electron from the TiNT valence band, forming a charge vacancy on the TiNT, which in turn oxidizes adsorbed hydroxyls to form hydroxyl radical, leading to acetaldehye oxidation.[15]

EPR spectroscopy was used to detail further the electronic properties of these materials. The chemically purified SWCNT gives an EPR spectrum consisting of Dysonian line-type signal with $g$ = 2.001 and peak-to-peak line width of $\Delta H_{app}$ = 23 G (Figure 10). This signal is characteristic of conduction band

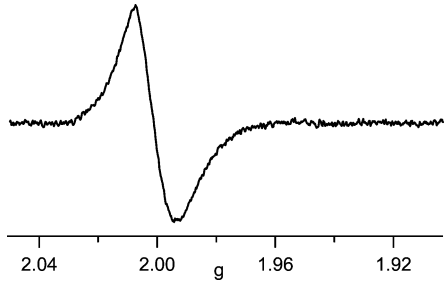


**Figure 10.** X-band EPR spectrum of SWCNTs recorded at 5 K. Instrument conditions: frequency 9.34 GHz, power 0.66 mW, modulation amplitude 2 G.

electrons[49] from either metallic (M) or narrow band gap semiconducting (SC) CNTs.[47,50,51] The electric arc discharge synthesis of SWCNTs is known to produce a mixture of both metallic and semiconducting tubes at a M/SC 1:2 ratio.[39,48]

For TiNT/SWCNT composites, the EPR spectrum shows a symmetric signal with $g$ = 2.003 and line width of $\Delta H_{app}$ = 3.8 G (Figure 11). The line shape and $g$ tensor value indicate

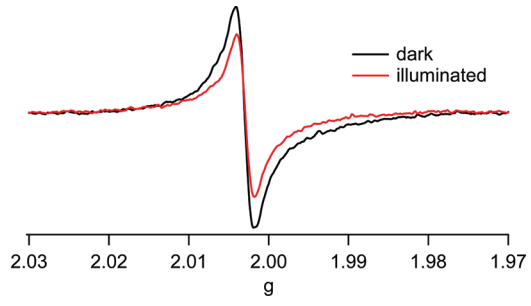


**Figure 11.** X-band EPR spectrum of 50NT/SWCNTs recorded at 5 K in the dark and under illumination using a Xe lamp and 440 nm cutoff filter. Instrument conditions: frequency 9.34 GHz, power 0.66 mW, modulation amplitude 2 G.

the presence of defect sites (in a form of carbon-centered radical) on the surface of SWCNTs. The presence of defects likely results in the formation of Ti−O−C centers. Upon visible light illumination, the intensity of the signal decreases, indicating that Ti−O−C centers participate in visible light absorption and result in efficient charge separation. The complete recovery of a signal was observed after 5 min in the dark, demonstrating a recombination of charges in the absence of reactants (Supporting Information Figure S4).

## CONCLUSION

A simple hydration−dehydration technique was used to synthesize TiNT/SWCNT composites, which showed enhanced activity in the photooxidation of acetaldehyde under UV and visible light in comparison with either conventional titania powders (P25) or titania nanotubes alone. Using a variety of techniques (SEM, TEM, XPS, Raman, PL, EPR) to characterize material features, we demonstrate that the TiNT/SWCNT composite possesses novel chemical, electronic, and optical properties. Under UV light, enhanced acetaldehyde decay was achieved as a result of electron transfer from the TiNT to the SWCNT, thereby diminishing rates of charge recombination. Visible light reactivity, however, is likely explained as the result of the band gap narrowing and charge-trapping effects of a variety of defect sites (oxygen vacacy/$Ti^{3+}$, Ti−C, Ti−O−C) created in synthesis. In addition, SWCNTs may also sensitize the titania nanotubes, initiating a sequence of electron transfers and ultimately creating reactive oxygen species, causing acetaldehyde decay. The degree of improved photoactivity depends on the relative mass ratio of the TiNT/SWCNT.

## ASSOCIATED CONTENT

### Supporting Information

TEM image of the titania nanotube, emission spectra of different lamps used for the photocatlytic degradation of acetaldehyde, table containing assignments of photoluminescence bands for titania nanotube, photoluminescence spectra with a 410 nm excitation, degradation of acetaldehyde in the absence of catalyst for different light sources, gas choromatogram trace showing $CO_2$ and acetaldehyde detection under photocatlytic reaction, X-band EPR spectrum of 50NT recorded at 5 K and, schematic representation of photocatalytic mechanisms are provided. This material is available free of charge via the Internet at http://pubs.acs.org.

## AUTHOR INFORMATION

### Corresponding Author

*E-mail: k-gray@northwestern.edu.

### Present Address

[#]Centre for Materials for Electronics Technology(C-MET), Nano Materials Division, Thrissur, Kerala, India.

## ACKNOWLEDGMENTS

This work was performed under the auspices of the U.S. Department of Energy, under Contracts DE-FG02-03 ER 15457/A003 and DE-AC02-06CH11357 (ICEP). D.F.−S. also acknowledges support from Honeywell Corp. Sample characterizations (XRD, SEM, Raman, XPS, and BET) were performed in the JB Cohen X-ray facility, and the NUANCE and Kung's Lab at Northwestern University.

## REFERENCES


(1) Shankar, K.; Basham, J. I.; Allam, N. K.; Varghese, O. K.; Mor, G. K.; Feng, X.; Paulose, M.; Seabold, J. A.; Choi, K.-S.; Grimes, C. A. *J. Phys. Chem. C* **2009**, *113*, 6327.
(2) Roy, S. C.; Varghese, O. K.; Paulose, M.; Grimes, C. A. *ACS Nano* **2010**, *4*, 1259.
(3) Adachi, M.; Murata, Y.; Harada, M.; Yoshikawa, S. *Chem. Lett.* **2000**, *29*, 942.
(4) Ghicov, A.; Schmuki, P. *Chem. Commun.* **2009**, 2791.
(5) Ou, H.-H.; Lo, S.-L. *Sep. Purif. Technol.* **2007**, *58*, 179.
(6) Yang, Y.; Zhong, H.; Tian, C. *Res. Chem. Intermed.* **2011**, *37*, 91.
(7) Asahi, R.; Morikawa, T.; Ohwaki, T.; Aoki, K.; Taga, Y. *Science* **2001**, *293*, 269.
(8) Vijayan, B. K.; Dimitrijevic, N. M.; Wu, J.; Gray, K. A. *J. Phys. Chem. C* **2010**, *114*, 21262.
(9) Liu, W.-X.; Ma, J.; Qu, X.-G.; Cao, W.-B. *Res. Chem. Intermed.* **2009**, *35*, 321.
(10) Mishra, A.; Banerjee, S.; Mohapatra, S. K; Graeve, O. A.; Misra, M. *Nanotechnology* **2008**, *19*, 445607.
(11) He, D.; Yang, L.; Kuang, S.; Cai, Q. *Electrochem. Commun.* **2007**, *9*, 2467.
(12) Ji, L.; Wang, Z.; Li, Z.; Liang, J. *Mater. Lett.* **2008**, *62*, 1979.
(13) Sun, J.; Gao, L. *J. Electroceram.* **2006**, *17*, 91.
(14) Gao, B.; Chen, G. Z.; Li Puma, G. *Appl. Catal., B* **2009**, *89*, 503.
(15) Wang, W.; Serp, P.; Kalck, P.; Faria, J. L. *J. Mol. Catal. A: Chem.* **2005**, *235*, 194.
(16) An, G. M.; Ma, W. H.; Sun, Z. Y.; Liu, Z. M.; Han, B. X.; Miao, S. D.; Miao, Z. J.; Ding, K. L. *Carbon* **2007**, *45*, 1795.
(17) Akhavan, O.; Abdolahad, M.; Abdi, Y.; Mohajerzadeh, S. *Carbon* **2009**, *47*, 3280.
(18) Gao, Y.; Liu, H. T.; Ma, M. J. *React. Kinet. Catal. Lett.* **2007**, *90*, 11.
(19) Llobet, E.; Espinosa, E. H.; Sotter, E.; Ionescu, R.; Vilanova, X.; Torres, J.; Felten, A.; Pireaux, J. J.; Ke, X.; Van Tendeloo, G.; Renaux, F.; Paint, Y.; Hecq, M.; Bittencourt, C. *Nanotechnology* **2008**, *19*, 375501.
(20) Yao, Y.; Li, G.; Ciston, S.; Lueptow, R. M.; Gray, K. A. *Environ. Sci. Technol.* **2008**, *42*, 4952.
(21) Woan, K.; Pyrgiotakis, G.; Sigmund, W. *Adv. Mater.* **2009**, *21*, 2233.
(22) Zhang, Y.; Tang, Z.-R.; Fu, X.; Xu, Y.-J. *ACS Nano* **2010**, *4*, 7303.
(23) Baiju, K. V.; Shukla, S.; Biju, S.; Reddy, M.; Warrier, K. G. K. *Catal. Lett.* **2009**, *131*, 663.
(24) Baiju, K. V.; Shukla, S.; Biju, S.; Reddy, M. L. P.; Warrier, K. G. K. *Mater. Lett.* **2009**, *63*, 923.
(25) Kasuga, T.; Hiramatsu, M.; Hoson, A.; Sekino, T.; Niihara, K. *Langmuir* **1998**, *14*, 3160.
(26) Kasuga, T.; Hiramatsu, M.; Hoson, A.; Sekino, T.; Niihara, K. *Adv. Mater.* **1999**, *11*, 1307.
(27) Yao, Y.; Li, G.; Gray, K. A.; Lueptow, R. M. *Langmuir* **2008**, *24*, 7072.
(28) Lee, S.-H.; Pumprueg, S.; Moudgil, B.; Sigmund, W. *Colloid Surf. B* **2005**, *40*, 93.
(29) Wang, Q.; Yang, D.; Chen, D.; Wang, Y.; Jiang, Z. *J. Nanopart. Res.* **2007**, *9*, 1087.
(30) Hurum, D. C.; Agrios, A. G.; Gray, K. A.; Rajh, T.; Thurnauer, M. C. *J. Phys. Chem. B* **2003**, *107*, 4545.
(31) Hurum, D. C.; Gray, K. A.; Rajh, T.; Thurnauer, M. C. *J. Phys. Chem. B* **2005**, *109*, 977.
(32) Suzuki, Y.; Yoshikawa, S. *J. Mater. Res.* **2004**, *19*, 982.
(33) Srikanta Swamy, S.; Calderon-Moreno, J. M.; Yoshimura, M. *J. Mater. Res.* **2002**, *17*, 734.
(34) Liu, G.; Zhao, Y.; Deng, K.; Liu, Z.; Chu, W.; Chen, J.; Yang, Y.; Zheng, K.; Huang, H.; Ma, W.; Song, L.; Yang, H.; Gu, C.; Rao, G.; Wang, C.; Xie, S.; Sun, L. *Nano Lett.* **2008**, *8*, 1071.
(35) Zhou, W.; Pan, K.; Qu, Y.; Sun, F.; Tian, C.; Ren, Z.; Tian, G.; Fu, H. *Chemosphere* **2010**, *81*, 555.
(36) Araña, J.; Doña-Rodríguez, J. M.; Tello Rendón, E.; Garriga i Cabo, C.; González-Díaz, O.; Herrera-Melián, J. A.; Pérez-Peña, J.; Colón, G.; Navío, J. A. *Appl.Catal., B* **2003**, *44*, 161.
(37) Dresselhaus, M. S.; Dresselhaus, G.; Jorio, A.; Souza Filho, A. G.; Saito, R. *Carbon* **2002**, *40*, 2043.
(38) Dechakiatkrai, C.; Chen, J.; Lynam, C.; Phanichphant, S.; Wallace, G. G. *J. Electrochem. Soc.* **2007**, *154*, A407.
(39) Ago, H.; Kugler, T.; Cacialli, F.; Salaneck, W. R.; Shaffer, M. S. P.; Windle, A. H.; Friend, R. H. *J. Phys. Chem. B* **1999**, *103*, 8116.
(40) Huang, Y.; Ho, W.; Lee, S.; Zhang, L.; Li, G.; Yu, J. C. *Langmuir* **2008**, *24*, 3510.
(41) Chen, L.-C.; Ho, Y.-C.; Guo, W.-S.; Huang, C.-M.; Pan, T.-C. *Electrochim. Acta* **2009**, *54*, 3884.
(42) Yu, H.; Quan, X.; Chen, S.; Zhao, H.; Zhang, Y. *J. Photochem. Photobiol. A: Chem.* **2008**, *200*, 301.
(43) Lawless, D.; Kapoor, S.; Meisel, D. *J. Phys. Chem.* **1995**, *99*, 10329.
(44) Shi, J.; Chen, J.; Feng, Z.; Chen, T.; Lian, Y.; Wang, X.; Li, C. *J. Phys. Chem. C* **2006**, *111*, 693.
(45) Liu, Z.; Zhang, X.; Nishimoto, S.; Murakami, T.; Fujishima, A. *Environ. Sci. Technol.* **2008**, *42*, 8547.
(46) Nishijima, K.; Ohtani, B.; Yan, X.; Kamai, T.-a.; Chiyoya, T.; Tsubota, T.; Murakami, N.; Ohno, T. *Chem. Phys.* **2007**, *339*, 64.
(47) Zhang, H.; Liu, S.; Wei, A.; He, Y.; Tang, X.; Xue, X.; Liang, L.; Wu, C. *J. Phys. Chem. Solids* **2000**, *61*, 1123.
(48) Cambré, S.; Wenseleers, W.; Goovaerts, E.; Resasco, D. E. *ACS Nano* **2010**, *4*, 6717.
(49) Wagoner, G. *Phys. Rev.* **1960**, *118*, 647.
(50) Thess, A.; Lee, R.; Nikolaev, P.; Dai, H.; Petit, P.; Robert, J.; Xu, C.; Lee, Y. H.; Kim, S. G.; Rinzler, A. G.; Colbert, D. T.; Scuseria, G. E.; Tománek, D.; Fischer, J. E.; Smalley, R. E. *Science* **1996**, *273*, 483.
(51) Chen, Y.; Chen, J.; Hu, H.; Hamon, M. A.; Itkis, M. E.; Haddon, R. C. *Chem. Phys. Lett.* **1999**, *299*, 532.